

Comparisons of CFD Simulations and In-service Data for the Self Propelled Performance of an Autonomous Underwater Vehicle

Alexander B Phillips, Stephen R Turnock
(University of Southampton, UK)

Maaten Furlong (National Oceanography Centre, Southampton, UK)

Abstract

A blade element momentum theory propeller model is coupled with a commercial RANS solver. This allows the fully appended self propulsion of the autonomous underwater vehicle Autosub 3 to be considered. The quasi-steady propeller model has been developed to allow for circumferential and radial variations in axial and tangential inflow. The non-uniform inflow is due to control surface deflections and the bow-down pitch of the vehicle in cruise condition. The influence of propeller blade Reynolds number is included through the use of appropriate sectional lift and drag coefficients. Simulations have been performed over the vehicles operational speed range ($Re = 6.8 \times 10^6$ to 13.5×10^6). A workstation is used for the calculations with mesh sizes up to 2×10^6 elements. Grid uncertainty is calculated to be 3.07% for the wake fraction. The initial comparisons with in service data show that the coupled RANS-BEMT simulation under predicts the drag of the vehicle and consequently the required propeller rpm. However, when an appropriate correction is made for the effect on resistance of various protruding sensors the predicted propulsor rpm matches well with that of in-service rpm measurements for vessel speeds (1m/s - 2m/s). The developed analysis captures the important influence of the propeller blade and hull Reynolds number on overall system efficiency.

1 Introduction

Autonomous Underwater Vehicles (AUV) are used for scientific research, military activities and commercial applications, Griffiths (2002). They have no external connections to the surface for powering, mission control or navigation. Increasing demand has led to the development of numerous commercial and academic AUV platforms over the past decade. Stevenson *et al.* (2007) note that many AUVs do not achieve the desired design speed and design range. This is attributed to under predicting drag, over predicting propulsive efficiency and overestimating the required mass of batteries.

The drag on an AUV or submarine can be found experimentally using towing tank tests, for example



Figure 1: Launch of the 7m Autonomous Underwater Vehicle Autosub

Thomas *et al.* (2003); Fallows (2004); Kimber and Marshfield (1993); Egeskov *et al.* (1994); Allen *et al.* (2000). Reynolds Averaged Navier Stokes (RANS) simulations have also been performed to determine the straight line resistance, simulations of bare asymmetric hull forms have been performed by Sarker *et al.* (1997) and Jagadeesh and Murali (2006). The appended straight line resistance of AUVs have been simulated by Phillips *et al.* (2007a); Seo *et al.* (2008) using commercial and academic RANS solvers. The determination of velocity based hydrodynamic derivatives of AUVs or submarine hull forms for manoeuvring models have been performed by Lee *et al.* (2005); Bodger and Dreyer (2006); Wu *et al.* (2005); Phillips *et al.* (2007b); Bellevre *et al.* (2000).

When considering the in-service performance of these vehicles the action of the propeller should be considered, since it modifies the surface pressure distribution and boundary layer flow at the stern of the vehicle with an associated change in hull resistance. Numerically the action of the marine propeller on the flow around a hull form can be included either by modelling explicitly the full rotating propeller in an unsteady RANS simulation of the hull-propeller system; or by modelling the hull with a propeller model based on an actuator-disc approach. A typical AUV propeller, like a ship model propeller, will often operate in the transition Reynolds No. range and use of a standard RANS approach may well not capture the behaviour of the propeller.

Nomenclature

$(1 + k)$	form factor	r_k	mesh refinement ratio
a	axial flow factor	R	resistance (N)
a'	circumferential flow factor	Re	Reynolds number
a''	race rotation factor due to tangential flow	t	thrust deduction factor
B	number of blades	T	thrust (N)
C	blade chord (m)	u_i	cartesian velocity components (m/s)
C_D	drag coefficient	U_∞	free stream velocity (m/s)
C_{DV}	volumetric drag coefficient	w	heave velocity (m/s)
C_L	lift coefficient	V_a	propeller advance velocity (m/s)
C_T	total drag coefficient	V_s	ship speed (m/s)
d	hull diameter (m)	w_T	Taylor wake fraction
D	propeller diameter (m)	x_i	cartesian co-ordinates (m)
J	advance coefficient	X	longitudinal force (N)
J_S	ship advance coefficient	Z	heave force (N)
k	reduced frequency $k = \omega C / 2U_\infty$	α	incidence angle (deg)
K	Goldstein correction factor	η_0	efficiency
K_Q	torque coefficient	η_D	propulsive efficiency
K_T	thrust coefficient	η_i	ideal efficiency
l	length (m)	η_H	hull efficiency
L	lift(N)	η_R	relative rotative efficiency
n	revolutions per second (s^{-1})	ρ	fluid density (kg/m^3)
M	pitch moment (Nm)	ϕ	hydrodynamic pitch (deg)
P	pressure (Pa)	Ψ	undisturbed flow angle (deg)
Q	torque(Nm)	ω	circular frequency (s^{-1})
r	local radius (m)	Ω	rotational velocity (s^{-1})

Schetz and Favin (1977) implemented an actuator disc propeller model within a RANS simulation; calculating the flow around a 2D section of the stern of an axisymmetric body. The propeller model allowed arbitrary variations in thrust distribution but swirl was assumed to be negligible. An increase in the u velocity component upstream and downstream of the model was observed. Stern *et al.* (1988) considered the flow over the stern of an axisymmetric body (Afterbody 1) with a propeller(4577). The use of prescribed and interactive bodyforce distributions where analysed using axial momentum terms, with and without swirl momentum. The prescribed body forces used thrust and moment distributions based on the radial circulation distributions presented by Hough and Ordway (1965). This method ignored the interaction of the propeller and hull. The interactive body force distribution calculated the propeller thrust and torque (K_T and K_Q) using a vortex lifting surface method was also demonstrated.

Nishi *et al.* (2007) used the commercial CFD code STAR-CD to simulate resistance and self propulsion tests on the AUV RAINBOW. The propeller is modelled using actuator disc theory and coupled with the RANS simulation to balance thrust and resistance. A reasonable correlation of the experimental and numer-

ical predictions of drag were found.

Bensow *et al.* (2004), performed Large Eddy Simulations (LES) of the flow around the DARPA Suboff at a $Re = 12 \times 10^6$. The source terms used to model the propeller were derived from a lifting line technique, this type of approach allows a realistic distribution of thrust and moment which is dependent on the inflow velocity.

Interactions between the hull and propulsor introduce an interaction velocity such that the total velocity at the propeller plane is due to the sum of the nominal wake velocity, propeller induced hull interaction velocity and the propeller's self induced velocity. The effective velocity, the sum of nominal wake and interaction velocity, is the input required for propeller analysis. Since the propeller loading and the effective wake are linked an iterative approach is required, Kim *et al.* (2008); Stern *et al.* (1988), to determine the correct inflow condition into the propeller model.

The use of propeller models results in the influence of the propeller being averaged over 1 revolution, consequently the blade frequency dependent effects such as tip and root vortices are not properly represented in the downstream wake. In order to capture their effects the blades must be modelled explicitly within the RANS simulation. Sreenivas *et al.* (2003) presented

RANS simulations of the flow around a generic appended axi-symmetric submarine hull fitted with the 5 bladed P-4381 propeller, using an unstructured mesh consisting of 12.4 million elements requiring a runtime of 26 hours on a wallclock using 32 processors.

RANS simulation of manoeuvring comes at a high computational cost due to the range of length and time scales that need to be captured. The time scales that must be considered range from a fraction of the propeller passage time to the length of the manoeuvre while the length scales vary from the length of the vessel down to the thickness of the boundary layer. Taylor *et al.* (1998) and Venkatesan and Clark (2007), have performed simulations of simple manoeuvres of the self propelled SUBOFF and ONR Body 1 respectively. Both model the propeller explicitly.

Although simulations with explicit propeller modelling are possible, propeller models based on actuator disc theory remain important for reducing the computational cost of RANS or LES simulations of manoeuvring self propelled marine vehicles. At the SIMMAN 2008 Workshop ed. Stern and Agdrup (2008), of the six self propelled calculations presented only one, Carica and Stern (2008), explicitly modelled the rotating propeller in a detached eddy simulation resulting in a CPU time of 200,000 hours.

In order to better understand the in-service performance of AUVs this work studies the self-propelled free flying condition of the AUV Autosub 3 using the commercial RANS solver ANSYS CFX V11. Derived results will be compared with in-service data and model scale experiments. The propeller will be modelled using an extended actuator disc approach using blade element momentum theory (BEMT) to determine the required axial and tangential momentum source terms. The eventual aim is to provide a cost-effective analysis technique for developing new AUVs.

2 Autosub 3

Autosub 3 (see Figure 1) is a large AUV (Length $\approx 7\text{m}$, Diameter 0.9m) developed by a team of engineers and oceanographers at the National Oceanography Centre, Southampton. Autosub has been employed in scientific research projects ranging from mapping manganese distributions in a sea loch, Statham *et al.* (2005), to under ice exploration in the Arctic and Antarctic, Wadhams *et al.* (2006).

Autosub 3 is a torpedo shaped AUV manoeuvred by four identical flapped control surfaces mounted at the rear of the vessel, in a cruciform arrangement, Figure 2. Two vertical rudders control the yaw of the vessel, while two horizontal sternplanes adjust the pitch. The full skeg foils use a NACA0015 section with a tip chord of 270mm, root chord of 368mm and a span of 386mm. The movable flap has a chord of 185mm and a span of

330mm.

The propulsion system consists of a single brushless DC motor that directly drives a two bladed aluminium alloy propeller, positioned at the rear of the vessel behind the control surfaces. The blades are 240mm long with a chord of 35mm, diameter 0.7m with a hub/diameter ratio of 0.3486, see Table 1 and Figure 2.

Table 1: Dimensions of Autosub Propeller

r/R	c/D	P/D
0.3143	0.0500	0.4905
0.3486	0.0500	0.5013
0.4171	0.0500	0.5160
0.4857	0.0500	0.5307
0.5543	0.0500	0.5453
0.6229	0.0500	0.5600
0.6914	0.0500	0.5747
0.7600	0.0497	0.5894
0.8286	0.0479	0.6041
0.8971	0.0438	0.6188
0.9657	0.0345	0.6334
1.0000	0.0194	0.5975



Figure 2: View Looking Aft over Autosub's stern, One Blade of the Propeller **AA** is Shown the Other is Obscured by the Hull

Most AUVs are ballasted prior to a mission with a slight positive buoyancy, Griffiths (2002). In the event of a system failure the vehicle will then rise gently to the surface. As a consequence to maintain its depth Autosub must use its control surfaces to adopt a nose down flying attitude, so a component of the thrust from the propeller and hydrodynamic lift from the hull can be used to oppose the buoyancy.

3 Blade Element Momentum Theory

Blade element momentum theory (BEMT) is commonly used in the design of wind turbines, Mikkelsen

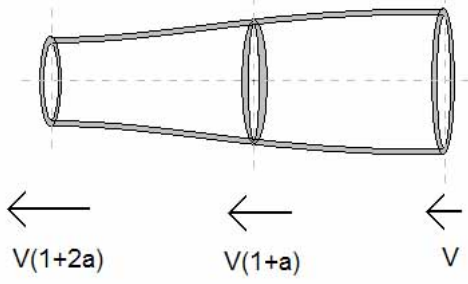


Figure 3: Momentum Theory

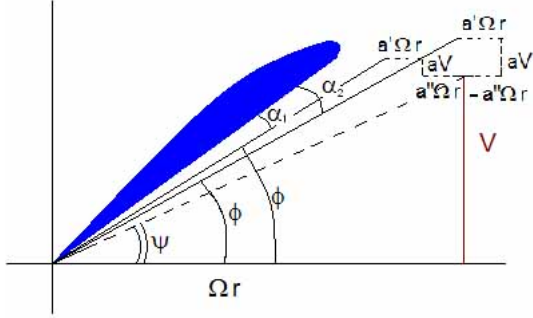


Figure 4: Blade Element Theory. α_1 is the Incidence Angle With $+a''$ while α_2 is the Incidence Angle with $-a''$

(2003); Burton *et al.* (2001), tidal turbines, Batten *et al.* (2006), and its importance for ship propellers is discussed in Benini (2004). The advantage of BEMT theory over more advanced methods is that it allows the lift and drag properties of the 2D section to be tuned to the local Reynolds number incorporating viscous effects such as stall or the effect of laminar separation at low Reynolds numbers.

In considering the flow down an annulus of radius r and thickness δr at the propeller disc, it can be shown that the increment of axial velocity at the disc is half that of downstream. The contribution to thrust at a given radius r can be written as: -

$$\frac{\delta T}{dr} = 4\rho\pi r V^2 K a(1+a), \quad (1)$$

where a is the axial flow factor and the factor K is the Goldstein correction to account for the propeller having a finite number of blades Goldstein (1929). Similarly the incremental torque can be written as:

$$\frac{\delta Q}{dr} = \rho 4\pi r^3 \Omega V K a'(1+a), \quad (2)$$

where Ω is the angular velocity of the propeller and a' is the circumferential inflow factor. The ideal efficiency η_i can be obtained from these equations as:

$$\eta_i = \frac{V \frac{dT}{dr}}{\Omega \frac{dQ}{dr}} = \frac{1-a'}{1+a}. \quad (3)$$

Non dimensionalising (1) & (2) results in: -

$$\frac{dK_T}{dr} = \pi J^2 x K a(1+a) \quad (4)$$

$$\frac{dK_Q}{dr} = \frac{1}{2} \pi^2 J x^3 K a'(1+a) \quad (5)$$

$$\frac{dL}{dr} = 1/2 \rho B C U^2 C_l(\alpha) \quad (6)$$

$$\frac{dD}{dr} = 1/2 \rho B C U^2 C_d(\alpha), \quad (7)$$

where B = number of blades, C = blade chord and the 2D lift and drag coefficients C_l and C_d depend on the angle of attack and are found experimentally or numerically for a 2D aerofoil. The section lift and drag are resolved to give the section torque and thrust:

$$\frac{dT}{dr} = \frac{dL}{dr} \cos\phi (1 - \tan\phi \tan\gamma) \quad (8)$$

$$\frac{dQ}{dr} = r \frac{dL}{dr} \cos\phi (\tan\phi + \tan\gamma). \quad (9)$$

These are combined to give a local section efficiency of:

$$\eta = \frac{\tan\Psi}{\tan(\phi + \gamma)} \quad (10)$$

In the nose down flight condition the angle of attack α is continuously changing as the blade rotates, leading to a cyclic variation in K_T and K_Q . This is included in the equations as a race rotation factor due to tangential flow a'' . a'' varies cyclically and is typically positive over one half of the revolution and negative over the other half.

Combining the ideal efficiency from momentum theory with the local efficiency from blade element theory the axial and circumferential inflow factors a and a' can be found at each section dr along the blade,

$$a' = 1 - \eta_i(1+a) \pm a'' \quad (11)$$

$$a = \frac{1 - \eta_i \pm a''}{\eta_i + \frac{1}{\eta} \tan^2\psi}. \quad (12)$$

The calculation of the inflow factors a and a' and the efficiency is solved iteratively to give section thrust and torque, equations 4 and 5.

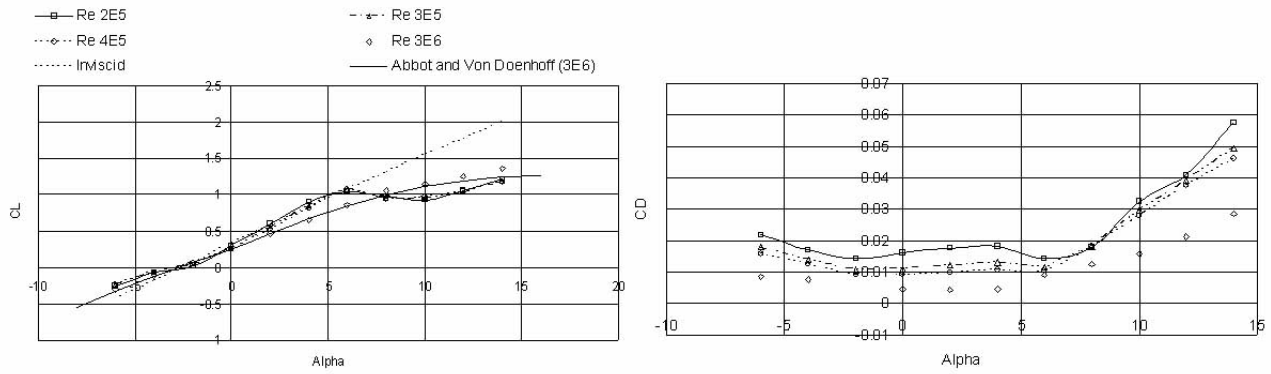


Figure 6: Lift and Drag Properties of NACA 65₂ – 415 Section

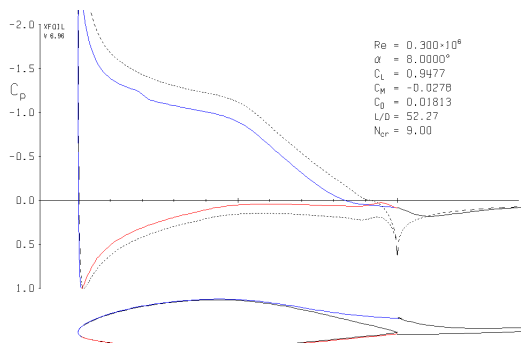


Figure 5: Pressure Distribution NACA 65₂ – 415 at 5° Incidence, XFOIL Output, Drela (1989)

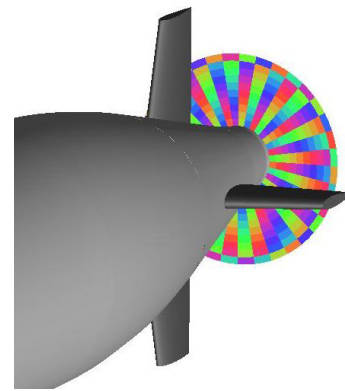


Figure 7: Subdivision of Propeller Disc, 36 Circumferential and 10 Radial

4 Blade Element Momentum Theory Implementation

The chord section shape for Autosub’s propeller is a modified NACA65₂ – 415. The performance of this section at a range of Reynolds numbers is presented in Figure 6, numerical predictions of 2D section performance are made using the 2D panel code XFOIL, Drela (1989). XFOIL is a linear vorticity stream function panel method with additional viscous boundary layer and wake models. The local section Reynolds number of the blades varies from around 200,000 at the root to 400,000 at the maximum chord (0.7D), then drops towards the tip with the local reduction in chord length. The performance of the section at these Reynolds numbers is shown in Figures 5 and 6. The foil experiences laminar separation from small incidence angles > 5°.

An existing compact BEMT code, Molland and Turnock (1996) has been modified to simulate the action of Autosub’s propeller. The 2D lift and drag data calculated from XFOIL has been modelled including the Reynolds number dependent drag coefficient.

When flying pitch down a non-uniform flow into the propulsor is observed leading to propeller sideforce as well as the normal thrust and moment loading. The propeller sideforce can lead to large moments due to the distance between the propeller and the Autosub centre of gravity (0.47L). In order to capture the radial and circumferential variation in propeller inflow conditions are determined for 360 discrete zones (10 radial divisions, 36 circumferential divisions), see Figure 7. The BEMT code is called for each of these locations to determine the local K_T and K_Q . This quasi-static approach is justified based on a reduced frequency of 0.00175, McCroskey (1982).

Within the RANS simulation the propeller is modelled as a cylindrical subdomain with a diameter equal to that of the propeller and a length equal to that of the rotating hub, 0.069D. Momentum source terms are then applied over the subdomain in cylindrical coordinates to represent the axial and tangential momentum induced by the propeller. An iterative approach described in Figure 8 is used to establish the self propulsion point.

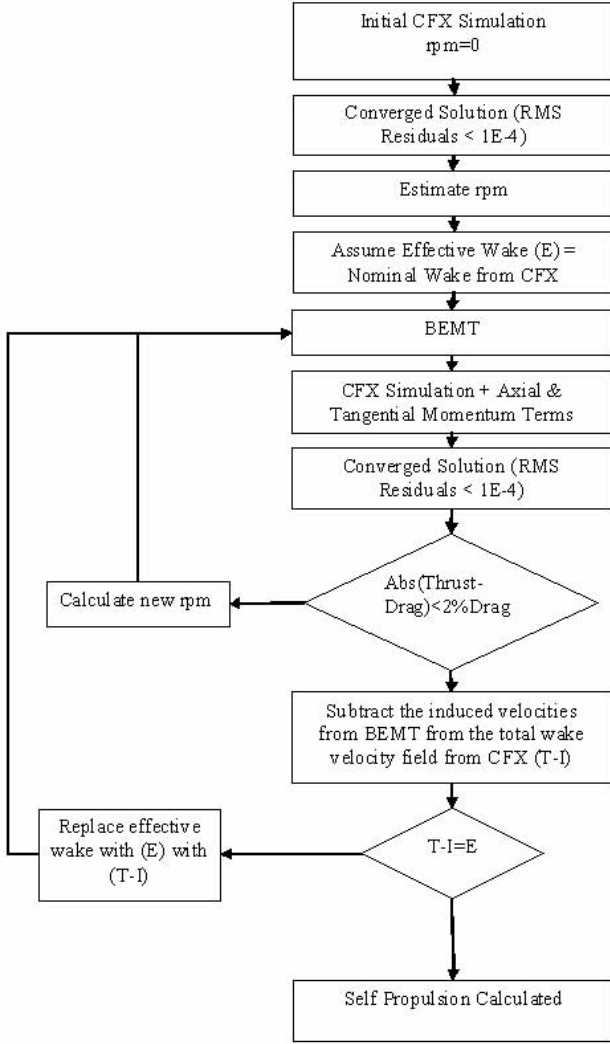


Figure 8: Flowchart Illustrating Self Propulsion Methodology. (T-I) Approach to Effective Wake Field Estimation modified from Carlton (2007) to show stages of analysis applied

This approach is implemented through the use of a CFX Junction Box Routine and CFX User Fortran Routines. The Junction Box routine is called at the end of every coefficient loop. It monitors convergence levels, extracts wake data and controls the set propeller rpm. The Fortran Routines are used to run the BEMT code based on the wake data and rpm from the Junction Box Routine, determine the momentum source distribution and return the source terms to CFX.

The computational cost of running the BEMT code at each coefficient loop is 0.1% of the cost of the RANS simulation.

4.1 Propeller open Water Performance

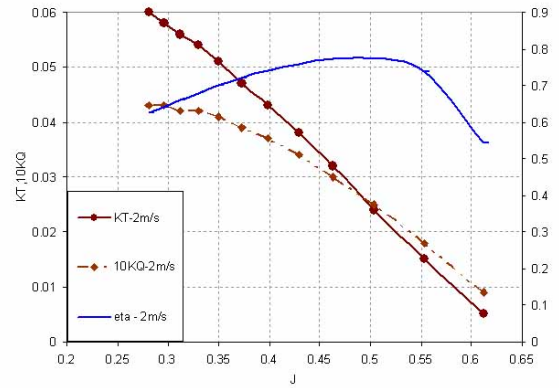


Figure 9: Autosub Propeller Open Water Performance

The open water performance of the propeller is presented in Figure 9 at an advance velocity of 2m/s. As the section drag is Reynolds number dependent for lower speeds there are small changes in thrust and larger increases in propeller K_Q . Unfortunately no open water performance data exist, however, the values obtained are similar to those predicted using the surface panel code, PALISUPAN, Turnock (1997) when the propeller was designed.

5 RANS

The fluid flow around the Autosub hullform has been modelled using the commercial finite volume code ANSYS CFX 11 (CFX), CFX (2006). The motion of the fluid is modelled using the incompressible (13), isothermal Reynolds Averaged Navier Stokes (RANS) equations (14) in order to determine the cartesian flow field ($u_i = u, v, w$) and pressure (p) of the water around the hull:

$$\frac{\partial \bar{U}_i}{\partial x_i} = 0 \quad (13)$$

$$\frac{\partial \bar{U}_i}{\partial t} + \frac{\partial \bar{U}_i \bar{U}_j}{\partial x_j} = -\frac{1}{\rho} \frac{\partial P}{\partial x_i} + \frac{\partial}{\partial x_j} \left\{ \nu \left(\frac{\partial \bar{U}_i}{\partial x_j} + \frac{\partial \bar{U}_j}{\partial x_i} \right) \right\} - \frac{\partial \overline{u'_i u'_j}}{\partial x_j} + f_i \quad (14)$$

Details of the computational approach are given in Table 2.

Table 2: Computational Machine and Solver Settings

Parameter	Setting
Computing	64-bit desktop pc 4 GB of RAM
Mesh Type	Structured Hexahedral
Turbulence Model	Shear Stress Transport, Menter (1994), with Scalable Wall Functions
Spatial Discretisation	High Resolution
Convergence Control	RMS of all residuals $< 10^{-4}$

5.1 Mesh Generation

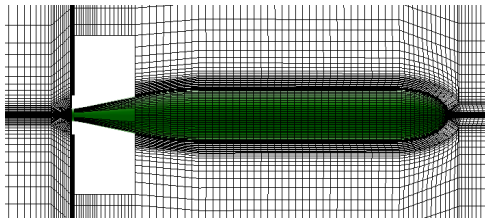


Figure 10: Hull Mesh (*medium*) Showing Cut Outs for Inserting Foil Mesh, Figure 11

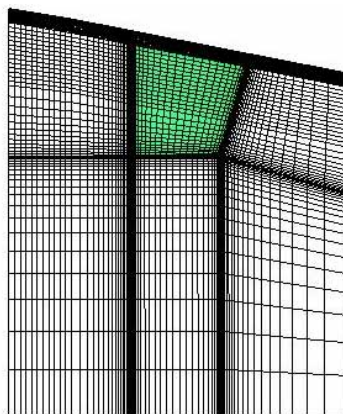


Figure 11: Foil Mesh (*medium*)

ANSYS CFX V11 does not allow the use of overlapping structured meshes, which have been used successfully to place refined meshes over control surfaces of

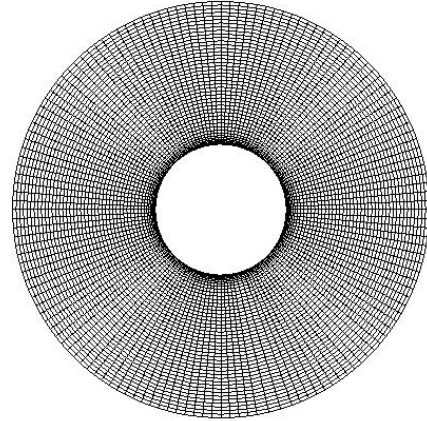


Figure 12: End View of Propeller Mesh (*medium*)

marine vehicles, for example Carrica *et al.* (2008); Kim *et al.* (2008); Venkatesan and Clark (2007). An alternative approach has been used which builds a structured mesh around the hull with blocks removed surrounding the control surfaces and the propeller cylinder, see Figure 10. Individual structured meshes are then generated for the two rudders (see Figure 11), the propeller (see Figure 12) and the fixed and movable parts of the sternplanes for a specific sternplane angle. These are then inserted into the main mesh. The meshes are joined by CFX General Grid Interface (CGI) connections, which allows the mesh density on each side of the interface to vary. By using this approach a higher mesh density can be achieved immediately around the control surfaces, without the need for small edges being continued to the domain boundaries, with resultant high aspect ratio elements.

A set of coarse, medium and fine meshes have been generated based on a mesh refinement ratio of $r_k = 2$, see Table 3, the y^+ parameter has been fixed by maintaining a constant first layer thickness for all the meshes. Five meshes were built for the movable sternplanes at 0, 3 and 6 degrees, the gap between the fixed and movable sections has been ignored.

Table 3: Typical Mesh Details at 2m/s

Mesh	Total No. Elements	y^+	No. Elements in Boundary Layer
Coarse	356466	70	6
Medium	976172	70	10
Fine	2365018	70	14

5.2 Boundary Conditions

An inlet boundary is placed 2l upstream, an outlet is placed 7l downstream and free slip walls are placed

2l away from the vehicle. For simulations without the propeller the longitudinal symmetry along the XZ axis was exploited, only half the vehicle was modelled with a symmetry boundary condition placed on the XZ plane.

5.3 Mesh Sensitivity

No suitable experimental results exist for validation of the straight line resistance or the wake fraction of Autosub. Grid based errors and uncertainties are estimated following Stern *et al.* (1999). Table 4 shows the grid convergence for the total resistance C_T , skin friction C_F , form factor $(1+k)$ and Taylor wake fraction w_T .

The total resistance, skin friction resistance and form factor demonstrate oscillatory convergence. The wake fraction demonstrates monotonic convergence, resulting in a grid uncertainty $U_G=3.07\%$ of the wake fraction on the finest mesh.

Table 4: Grid Convergence

Variable	Fine (SG)	Medium	Coarse
$C_T \times 1000$	3.285	3.260	3.488
$C_F \times 1000$	2.818	2.821	2.777
$(1+k)$	1.166	1.156	1.256
w_T	0.173	0.177	0.187

6 Results

6.1 Global Loads

The global loads acting on the vessel are non-dimensionalised by the length of the vehicle (L) the velocity of the vehicle (V) and the density of the fluid (ρ), a prime symbol is used to signify the non dimensional form for example:

$$v' = \frac{v}{V}, Y' = \frac{Y}{1/2\rho L^2 V^2}, N' = \frac{N}{1/2\rho L^3 V^2} \quad (15)$$

The forces and moments generated by the rudder are presented in figures 16, 17 and 18. The results are compared with experimental data from Kimber and Marshfield (1993) for the Autosub DTV (5.2m scale model). The numerical simulations compare well with the experimental results for heave force and pitch moment. The numerical drag predictions correspond well with the average of positive and negative heave velocities.

6.2 Nominal Wake

The propulsor on an AUV usually operates partly or entirely inside the hull boundary layer. As a consequence the prediction of the inflow into the propeller

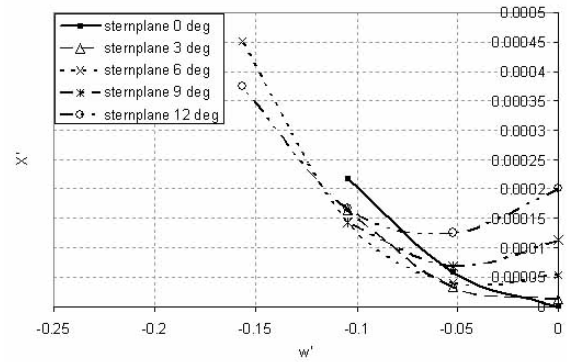


Figure 13: Surge Force (X') Versus Heave Velocity (w')

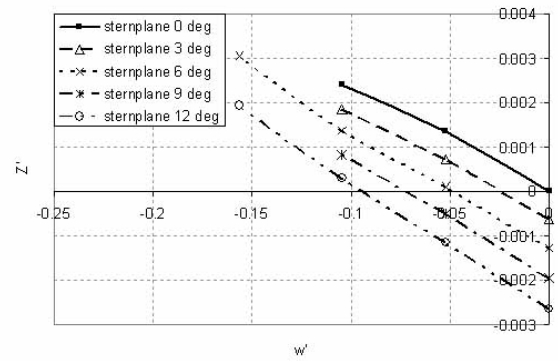


Figure 14: Heave Force (Z') Versus Heave Velocity (w')

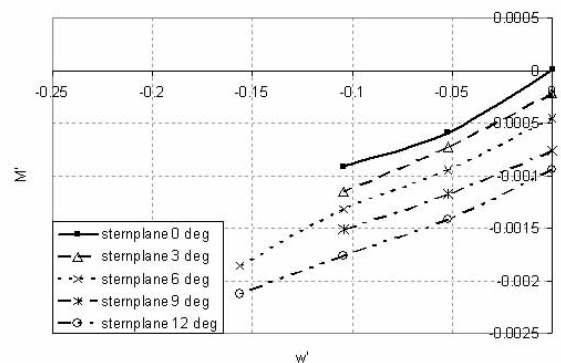


Figure 15: Pitch Moment (M') Versus Heave Velocity (w')

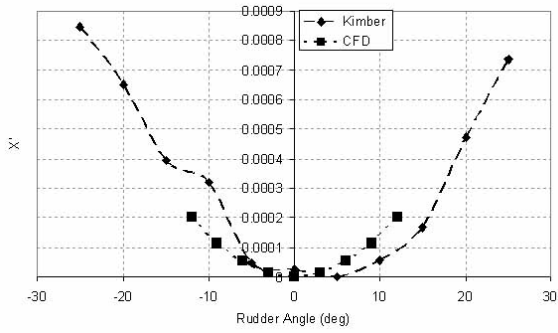


Figure 16: Surge Force (X') Versus Sternplane Angle

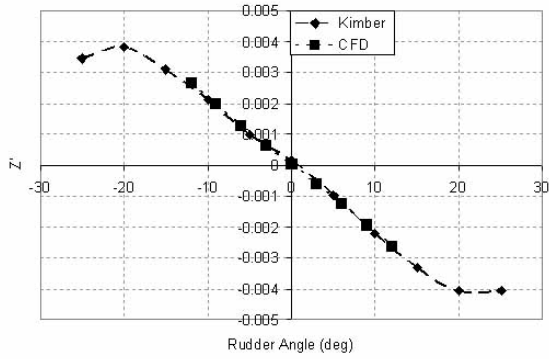


Figure 17: Heave Force (Z') versus Sternplane Angle

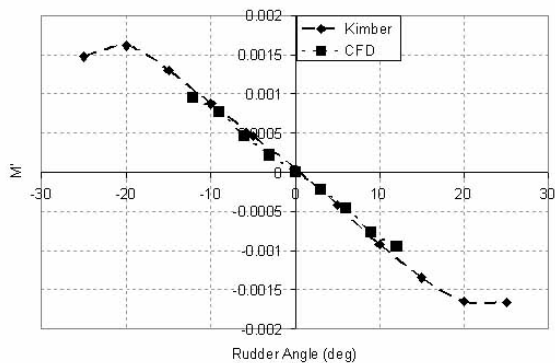


Figure 18: Pitch Moment (M') Versus Sternplane Angle

plane is dependent on good modelling of the growth of the boundary layer of the hull and that of the wake of any appendages forward of the propulsor. As the vehicle undergoes a manoeuvre the flow around the hull is modified, changing the propeller inflow and its performance. No experimental wake data exists for Autosub however the form of the wake pattern at 0° pitch & 0° sternplane resembles that measured behind the DARPA Suboff when fitted with 4 control surfaces in a cruciform arrangement, Huang *et al.* (1992).

The viscous wake due to the boundary layer on the control surfaces is observed as a cruciform of slower moving fluid in the propeller wake. Pairs of counter rotating vortices generated at the root of the control surfaces convect downstream, bringing higher momentum fluid down onto the hull either side of the control surfaces.

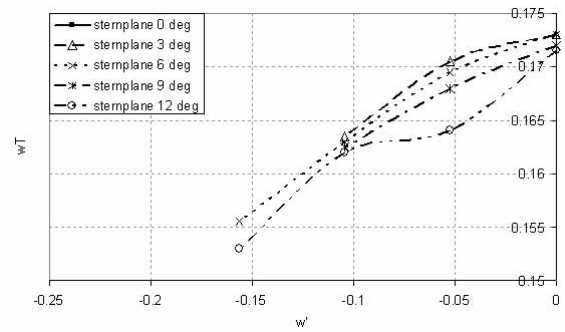


Figure 19: Influence of Pitch and Sternplane Angle on Wake Fraction (w_T)

Figure 19 and 20 illustrate the variation in the propeller wake at a series of nose down pitch angles and rudder angles. As the drift angle increases crossflow around the hull leads to an increase in the average u velocity in the propeller plane this overcomes the $\cos\theta$ effect and leads to a reduction in the wake fraction.

7 Self Propulsion

Due to the iterative nature of the solution process for the self propelled cases the medium mesh has been used in these studies to retain a solution time of less than 24 hours wall time.

The iterative loop between the RANS solver and BEMT code is repeated until the self-propulsion point of the vehicle is found ($T = (1 + t)R$). Table 5 shows the history of the propeller rpm selection used to determine the self propulsion point of the vehicle for the 2m/s case based on the initial nominal wake. After four rpm selections the self propulsion point has been determined. Further stages are subsequently performed to determine the self propulsion point based

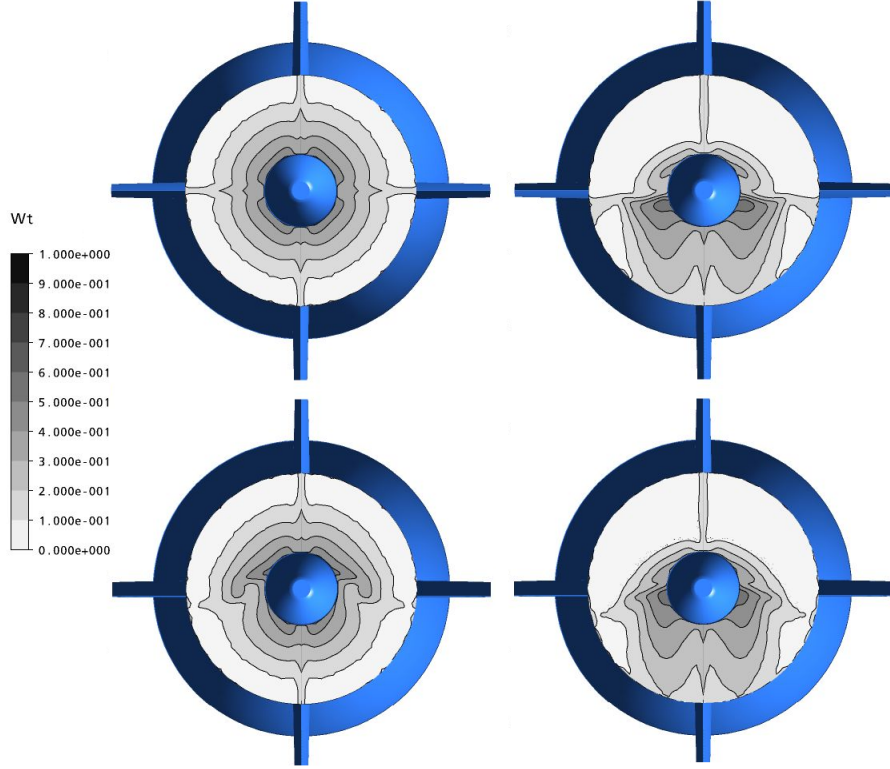


Figure 20: Wake Contours at the Propeller Disc for 0° pitch & 0° sternplane (top left), 6° pitch & 0° sternplane (top right), 0° pitch & 6° sternplane (bottom left), 6° pitch & 6° sternplane (bottom right)

on the modified wake due to the propeller with an updated input to the BEMT code.

Table 5: RPM Selection to Achieve Self-Propulsion with Nominal Wake

Stage	RANS	BEMT			$ E $	
	$C_T \times 1000$	n	J_s	K_T		$10K_Q$
0	3.260	0.00	0.00	0.000	0.000	100.0
1	3.566	5.00	0.57	0.024	0.023	15.5
2	3.375	4.28	0.67	0.009	0.012	65.9
3	3.530	4.86	0.59	0.022	0.021	1.4

Figure 21 illustrate the nominal, effective and total velocities components at the propeller plane. Since the operational thrust loading of the Autosub propeller is small, $K_T/J^2 = 0.07$, the velocities induced by the propeller are small, approximately 10% of the nominal velocity, similarly the induced velocities are likewise small.

Table 6 shows the self propulsion parameters for Autosub at 1m/s, 1.5m/s and 2m/s in level flight, efficiencies have been calculated using the thrust identity method. The measured K_T and K_Q at the self propul-

sion point decrease with increasing propeller Re due to the reduction in local section drag coefficient C_D . Since K_Q is more dependent on local section C_D propeller efficiency increases with propeller Re . The wake fraction w_T reduces at increasing Autosub Reynolds number, this corresponds to the reduction in boundary layer thickness. The reduction in wake fraction with Re is greater than the corresponding reduction in thrust deduction leading to a decrease in hull efficiency η_H with increasing Autosub Reynolds number.

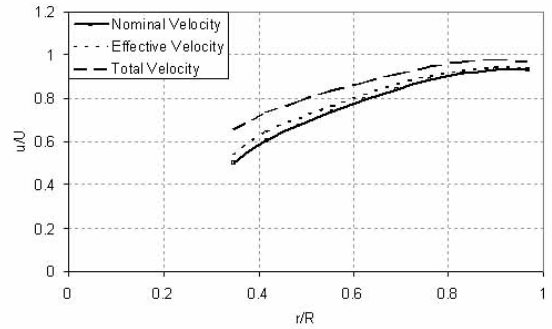


Figure 21: Nominal, Effective and Total Velocity Components in the Propeller Plane

Table 6: Self Propulsion Parameters

Parameter	Forward Speed		
	1m/s	1.5m/s	2m/s
Autosub Re	6793000	10189500	13586000
Propeller Tip Re	74593	128371	169391
J_S	0.5719	0.5751	0.5831
K_T	0.0232	0.0220	0.0216
$10K_Q$	0.0243	0.0224	0.0216
η_0	0.7161	0.7825	0.7886
η_R	1.0712	1.0277	1.0068
t	0.0878	0.0866	0.0835
w_T	0.1919	0.1629	0.1585
η_H	1.1287	1.0912	1.0891
η_D	0.8658	0.8776	0.8647

7.1 Flight

Depth control on Autosub 3 is performed using a cascade design, with pitch control as the inner loop and depth control as the outer, see Figure 22. Figure 23 shows how the sternplane angle is varied with forward speed, at slower speeds a larger stern plane angle is required to generate sufficient pitching moment to overcome the hydrostatic restoring moment, \overline{BG} , in order to achieve the required pitch angle to maintain level flight.

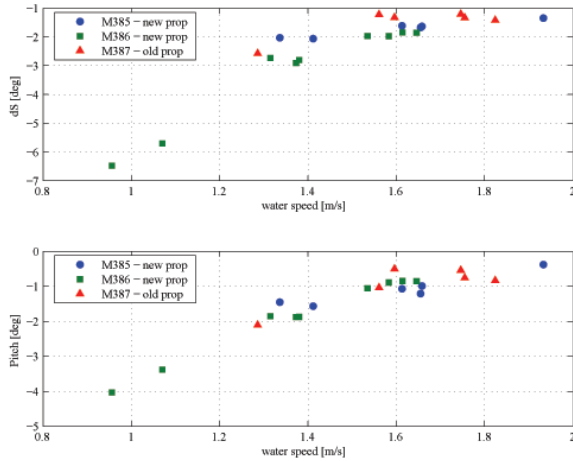


Figure 22: Variation in Stern Plane Angle (dS) and Pitch Angle Versus Flying Speed, (*Mission data from Autosub Missions 385, 386 and 387*)

Using the mission data from Figure 22 the flight condition at 1m/s (nose down pitch angle of 4° and a sternplane angle of -6°) has been simulated using the coupled RANS-BEMT.

Figure 24 illustrates the flow around the vehicle. Crossflow around the hull results in slower moving fluid from the sternplane and hull boundary layers being forced downwards. This non uniform inflow into

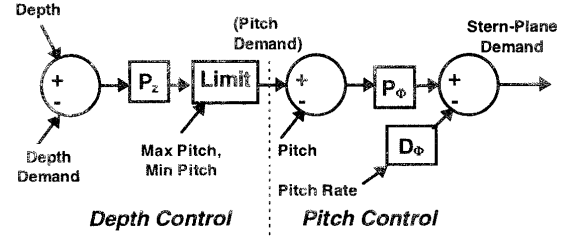


Figure 23: Autosub Depth Control Algorithm, McPhail and Pebody (1997)

the propeller leads to radial and circumferential variation in thrust and torque coefficients, see Figure 25 and 26, δK_T and δK_Q values fluctuate by more than 50% over 1 revolution. The flow is accelerated by the action of the propeller which imparts a clockwise swirl component into the wake.

In averaging the velocity components over the 360 segments the more extreme fluctuations may have been reduced, further studies are required to determine a suitable number of subdivisions.

In pitching the vehicle nose down the thrust required has increased by 13.6%, requiring an increase in rpm of 3.8%. The torque distribution results in a propeller side force of 1.43N which causes a yawing moment of 4.69Nm which would require a 2° rudder angle to correct. This compares well with in-service measured data.

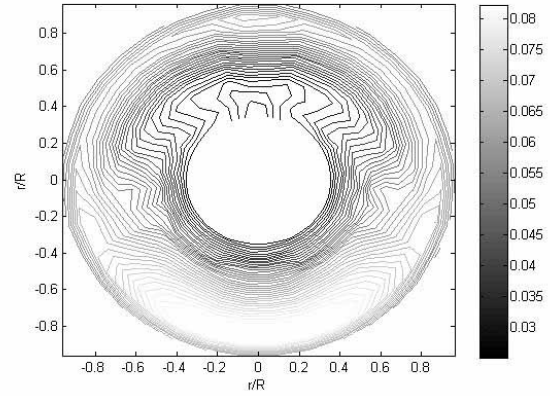


Figure 25: Contour Plot Showing Variation in Local δK_T Values over the Propeller Disc

8 Comparison with trial data

The coupled RAN-BEMT simulation estimates a propeller rpm of 294 for self propulsion at 2m/s. This value is substantially lower than the rpm values seen in-service, Figure 27. There are two possible causes of

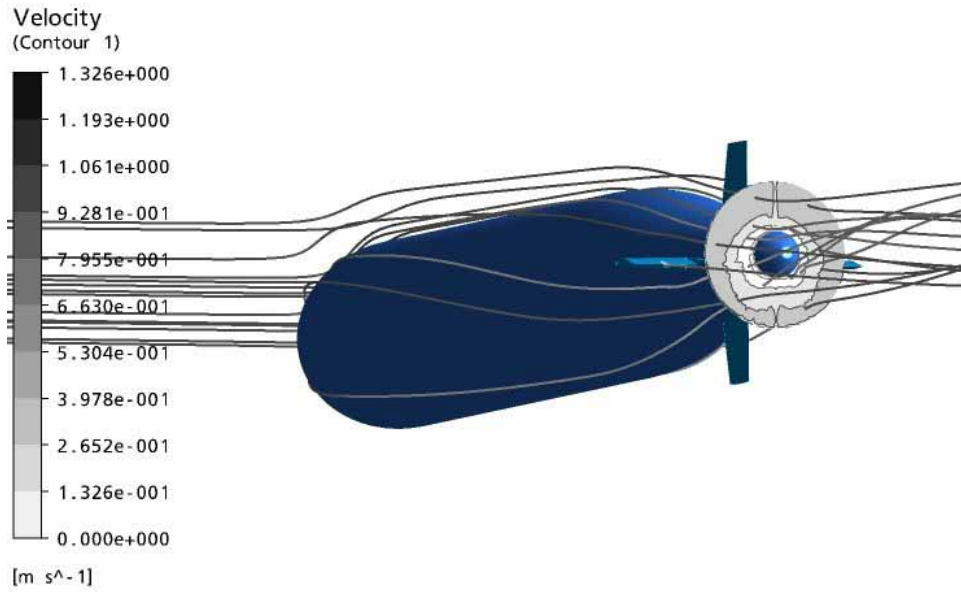


Figure 24: Streamlines around the Vehicle at a Nose Down Pitch Angle of 4° and a Sternplane Angle of -6°

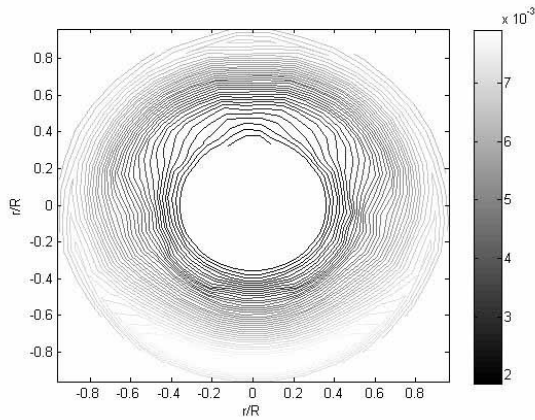


Figure 26: Contour Plot Showing Variation in Local δK_Q Values over the Propeller Disc

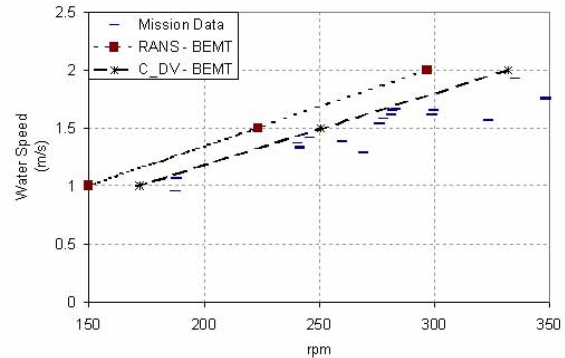


Figure 27: RPM versus water speed, (*Mission data from Autosub Missions 385, 386 and 387*)

Furlong (2005).

this discrepancy; over prediction of K_T in the BEMT code or under prediction of the vehicle drag in the RANS simulation.

Using the ITTC 57 correlation line (16), and a form factor from Hoerner (1965) for a streamlined body as a function of vessel length (l) and diameter (d), (17) the bare hull drag coefficient can be estimated as $C_{DV} = 0.02219$ compared with $C_{DV} = 0.0215$ derived from the RANS simulation. The four control surfaces add an extra 13% to the drag leading to a $C_{DV} = 0.024$, lower than the accepted value for Autosub derived from deceleration tests of $C_{DV} = 0.045$,

$$C_{F_{1957}} = \frac{0.075}{(\log(R_e) - 2)^2} \quad (16)$$

$$(1 + k) = 1 + 1.5(d/l)^{3/2} + 7(d/l)^3 \quad (17)$$

The discrepancies between the numerical and in service drag is believed to be due to the various instruments and antennae with project through Autosub’s hull, see Figure 1, these protuberances have been ignored in the numerical simulations. Allen *et al.* (2000) performed towing tank tests to determine the relative contribution of hull, fins, transducers and nose pockets to the total hydrodynamic drag of a REMUS AUV.

The results identified the transducer and nose pockets comprised nearly half of the total drag of the vehicle. Thus highlighting that the drag of the basic hull is often not the major contributor to the total drag of an AUV.

Taking the wake fraction and thrust deduction calculated by the RANS-BEMT simulation, and replacing the drag calculated from the RANS analysis with that calculated using the drag coefficient $C_{DV} = 0.045$ the resulting prediction of rpm versus water speed are presented on Figure 27. These show good agreement with the in service data confirming the analysis undertaken.

9 Conclusions

A robust and rapid method of coupling a Blade Element Momentum theory code for marine propellers with the commercial RANS code ANSYS CFX is presented. The computational cost of running the BEMT code at each coefficient loop is 0.1% of the cost of the RANS simulation, and thus significantly lower than modelling the propeller blade in the RANS simulation explicitly. Viscous effects such as stall or low Re effects such as laminar separation can be included when defining the lift and drag properties of the 2D sections.

Radial and circumferential variation in propeller performance can be captured by considering the local inflow conditions at a series of radial and circumferential divisions. This allows for non uniform propeller inflow such as that observed behind a ship or submarine.

Self propulsion simulations using the RANS-BEMT method have been performed over the range of operational Reynolds numbers for the AUV Autosub 3. Hull efficiency is shown to decrease with Reynolds number while the propeller open water efficiency increases. Comparisons with in service data show the RANS-BEMT simulation under predicts the drag of the vehicle and consequently the required rpm. This is attributed to the various instruments and antennae which protrude through the hull which are not included in the CFD analysis. After correcting for the drag of the protuberances the predicted rpm show fair correlation with the in-service data.

In comparing the results for level flight at 1m/s with the true nose down flying attitude lead to the required thrust increasing by 13.6%, requiring an increase in rpm of 3.8% and a power increase of 11.9%.

The low computational cost of the propeller model combined with its ability to consider non-uniform and tangential inflow conditions make it suitable for use in future transient manoeuvring simulations.

Acknowledgements

The authors gratefully acknowledge the support of the School of Engineering Sciences and the National Oceanography Centre, Southampton in funding the PhD research of Mr A.B. Phillips as part of the on-going development programme of future AUVs for oceanographic exploration.

References

- B. Allen, W. S. Vorus, and T. Presreo. Propulsion system performance enhancements on REMUS AUVs. In *OCEANS 2000 MTS/IEEE Conference and Exhibition*, volume 3, pages 1869–1873, 2000.
- W.M.J. Batten, A.S. Bahaj, A.F. Molland, and J.R. Chaplin. Hydrodynamics of marine current turbines. *Renewable Energy*, 31:249–256, 2006.
- D. Bellevre, A. Diaz de Tuesta, and P. Perdon. Submarine manoeuvrability assessment using computational fluid dynamic tools. In *In Proc. 23th Symposium on Naval Hydrodynamics, Val de Reuil, France*, pages 820–832, September 2000.
- E. Benini. Significance of blade element theory in performance prediction of marine propellers. *Journal of Ocean Engeneering*, 31:957–974, 2004.
- R.E. Bensow, T. Persson, C. Fureby, U. Svennberg, and N. Alin. Large eddy simulation of the viscous flow around submarine hulls. In *25th Symposium on Naval Hydrodynamics*, 2004.
- D. Bodger and J. Dreyer. Prediction of hydrodynamic forces and moments for underwater vehicles using overset grids. In *Proceedings of AIAA Aerospace Meeting and Exhibit Reno, Nevada, jan 9-12, 2006*.
- T. Burton, D. Sharpe, N. Jenkins, and E. Bossanyi. *Wind Energy : Handbook*. Chichester : Wiley, 2001., 2001.
- J. Carlton. *Marine Propellers and Propulsion*. Butterworth-Heinemann, 2nd edition edition, 2007.
- P.M. Carrica and F. Stern. DES simulations of KVLCC1 in turn and zigzag maeuvers with moving propeller. In *SIMMAN 2008 Workshop on Verification and Validation of Ship Manoeuvring Simulation Methods, Copenhagen April 14th-16th*, 2008.
- P.M. Carrica, F. Ismail amd M. Hyman, S. Bushan, and F. Stern. Turn and zigzag maneuveres of a surface combatant using a URANS approach with dynamic overset grids. In *SIMMAN 2008 Workshop on Verification and Validation of Ship Manoeuvring Simulation Methods, Copenhagen April 14th-16th*, 2008.

- ANSYS CFX. *ANSYS CFX, Release 11.0*. ANSYS, 2006.
- M. Drela. XFOil: an analysis and design system for low reynolds number airfoils. In *Conference on low Reynolds number airfoil aerodynamics, University of Notre Dame*, 1989.
- P. Egeskov, A. Bjerrum, A. Pascoal, C. Silvestre, C. Aage, and L.W.; Smitt. Design, construction and hydrodynamic testing of the AUV MARIUS. In *Autonomous Underwater Vehicle Technology, 1994. AUV '94., Proceedings of the 1994 Symposium on, 19-20 July 1994*.
- C. D. Fallows. *Characterisation of the Propulsion System of Autonomous Underwater Vehicles*. PhD thesis, University of Southampton, 2004.
- M. Furlong. Deceleration trials analysis. Technical report, Underwater Systems Laboratory, National Oceanography Centre, Southampton, 2005.
- S. Goldstein. On the vortex theory of screw propellers. In *proceedings of the Royal Society*, 1929.
- G. Griffiths. *Technology and Applications of Autonomous Underwater Vehicles*. Taylor and Francis, 2002.
- S.F. Hoerner. *Fluid Dynamic Drag*. Published by the Author, 1965.
- G. R. Hough and D. E. Ordway. The generalised actuator disc. *Developments in Theoretical and Applied Mechanics*, 2:317–336, 1965.
- T. T. Huang, H-L. Liu, N.C. Groves, T. J. Forlini, J.N. Blanton, and S. Gowing. Measurements of flows over an axisymmetric body with various appendages (DARPA SUBOFF experiments). In *Proceedings of the 19th Symposium on Naval Hydrodynamics. Seoul, Korea, August 1992*.
- P. Jagadeesh and K. Murali. Investigations on alternative turbulence closure models for axisymmetric hull-forms. *The Journal of Ocean Technology*, 1(11):37–57, Autumn 2006.
- S. Kim, J. Kim, I. Park, G. Kim, and S. Van. High fidelity RANS simulation for a self-propelled ship in model scale. In *RINA Marine CFD, Southampton 26th 27th March, 2008*.
- N. Kimber and W. Marshfield. Design and testing of control surfaces for the Autosub Demonstrator Test Vehicle. Technical report, DRA Haslar, 1993.
- S. Lee, E. Jin, and H. Lee. Evaluation of the vertical plane stability by CFD. In *Proceedings of the fifteenth(2005) International Polar Engineering Conference, Soeul Korea, June 19-24 2005*.
- WJ McCroskey. Unsteady airfoils. *Ann Rev Fluid Mech*, 14:285311, 1982.
- S.D. McPhail and M. Pebody. Autosub-1. a distributed approach to navigation and control of an autonomous underwater vehicle. In *7th International Conference on electronic Engineering in Oceanography, 23-25 June 1997, 1997*.
- F.R. Menter. Two-equation eddy-viscosity turbulence models for engineering applications. *AIAA Journal*, 32(8):1598 – 605, 1994. ISSN 0001-1452.
- Robert Mikkelsen. *Actuator Disc Methods Applied to Wind Turbines*. PhD thesis, Department of Mechanical Engineering Technical University of Denmark, 2003.
- A. F. Molland and S. R. Turnock. A compact computational method for predicting forces on a rudder in a propeller slipstream. In *Transactions of RINA*, volume 138, pages 59–71, 1996.
- Y. Nishi, M. Kashiwagi, W. Koterayama, M Nakamura, Z. Z. H. Samual, I Yamamoto, and T. Hyakumdome. Resistance and propulsion performance of an underwater vehicle estimated by a CFD method and experiment. In *Proceedings of the seventeenth (2007) International Offshore and Polar Engineering Conference, Lisbon Portugal, July 1-6 2007*.
- A. B. Phillips, M. Furlong, and S.R. Turnock. The use of computational fluid dynamics to assess the hull resistance of concept autonomous underwater vehicles. In *Oceans'07, Aberdeen, 2007a*.
- A. B. Phillips, M. Furlong, and S.R. Turnock. The use of computational fluid dynamics to determine the dynamic stability of an autonomous underwater vehicle. In *10th Numerical Towing Tank Symposium, Hamburg, 2007b*.
- T. Sarker, P.G. Sayer, and S.M. Fraser. A study of autonomous underwater vehicle hull forms using computational fluid dynamics. *International Journal for Numerical Methods in Fluids*, 25:1301–1313, 1997.
- J.A. Schetz and S. Favin. Numerical solution for the near wake of a body with a propeller. *Journal of Hydraulics*, 11:136–141, 1977.
- C. C. Seo, Jo. G, and H. S. Choi. Control simulations of an underwater glider using CFD analysis. In *OCEANS'08 MTS/IEEE KOBE-TECHNO-OCEAN '08 (OTO'08)*, 2008.
- K. Sreenivas, A. N. Cash, D. G. Hyams, and L.K. Taylor. Computational study of propulsor-hull interactions. In *41st Aerospace Sciences Meeting and Exhibit, 6-9 January 2003*.

- P.J. Statham, D.P. Connelly, C.R. German, T. Brand, J.O. Overnell, E. Bulukin, N. Millard, S. McPhail, M. Pebody, J. Perrett, M. Squire, P. Stevenson, and A. Webb. Spatially complex distribution of dissolved manganese in a fjord as revealed by high-resolution in situ sensing using the autonomous underwater vehicle Autosub. *Environmental Science and Technology*, 2005.
- F. Stern and K. Agdrup. SIMMAN 2008 workshop on verification and validation of ship manoeuvring simulation methods. In *Draft Workshop Proceedings*, 2008.
- F. Stern, H. T. Kim, N. M. Patel, and H. C. Chen. A viscous-flow approach to the computation of propeller-hull interaction. *Journal of Ship Research*, 32:246–262, 1988.
- F. Stern, R. V. Wilson, H. W. Coleman, and E. G. Paterson. Verification and validation of CFD simulations. Technical Report IIHR Report No. 407, Iowa Institute of Hydraulic Research, September 1999.
- P. Stevenson, M. Furlong, and D. Dormer. AUV shapes - combining the practical and hydrodynamic considerations. In *Oceans '2007 Conference Proceedings*, 2007.
- L.K. Taylor, R. Pankajakshan and M. Jiang, C. Sheng, W.R. Briley, D.L. Whitfield, F. Davoudzadeh, A. Bger, and H. J. Gibeling. Large-scale simulations for maneuvering submarines and propulsors. In *29th Plasmadynamics and Lasers Conference, Albuquerque, June 15-18*, 1998.
- R. Thomas, N. Bose, and C. D. Williams. Propulsive performance of the autonomous underwater vehicle 'C-Scout'. In *Oceans '2003 Conference Proceedings*, 2003.
- S.R. Turnock. Technical manual and user guide for the surface panel code: Palisupan. Technical report, University of Southampton, Southampton, UK (Ship Science Reports, 100), 1997.
- G. Venkatesan and W. Clark. Submarine maneuvering simulations of ONR Body 1. In *Proceedings of 26th International Conference on Offshore Mechanics and Arctic Engineering*, 2007.
- P. Wadhams, J.P. Wilkinson, and S.D. McPhail. A new view of the underside of Arctic sea ice. *Geophysical Research Letters*, 2006.
- B. Wu, X. Fu, X. Kuang, and O. Q. Mia. Investigation of hydrodynamic characteristics of submarine moving close to the sea bottom with CFD methods. *Journal of Ship Mechanics*, 9, 2005.